RNASEH1 mutations impair mtDNA replication and cause adult-onset mitochondrial encephalomyopathy

Aurelio Reyes[1], Laura Melchionda[2], Alessia Nasca[2], Franco Carrara[2], Eleonora Lamantea[2], Alice Zanolini[2], Costanza Lamperti[2], Mingyan Fang[3], Jianguo Zhang[3], Dario Ronchi[4], Sara Bonato[4], Gigliola Fagiolari[5], Maurizio Moggio[5], Daniele Ghezzi[2*], Massimo Zeviani[1*]

[1]Mitochondrial Biology Unit, Medical Research Council, Cambridge CB2 0XY, UK; [2]Foundation Carlo Besta Neurological Institute-IRCCS, Unit of Molecular Neurogenetics, Milan 20126, Italy; [3]Beijing Genomic Institute, Shenzhen 518083, China; [4]Neurology and [5]Neuromuscular Units, Neuroscience Section, Department of Pathophysiology and Transplantation, Dino Ferrari Center, IRCCS Foundation Ca' Granda Ospedale Maggiore Policlinico, University of Milan, Milan 20122, Italy.

*Correspondence to:

Daniele Ghezzi, PhD

Unit of Molecular Neurogenetics

Foundation Carlo Besta Neurological Institute

Via Libero Temolo, 4

20126 Milan, Italy

daniele.ghezzi@istituto-besta.it

Massimo Zeviani, MD, PhD

MRC Mitochondrial Biology Unit

Wellcome Trust/MRC Building

Hills Road

Cambridge

CB2 0XY

UK

Tel: +44 (0)1223 252702

Fax: +44 (0)1223 252705

mdz21@mrc-mbu.cam.ac.uk

office +44(0)1223252702

ABSTRACT

Chronic progressive external ophthalmoplegia (CPEO) is common in mitochondrial disorders, being frequently associated with multiple mtDNA deletions. The onset is typically in adulthood and affected subjects may also present general muscle weakness. The underlying genetic defects comprise autosomal dominant or recessive mutations in several nuclear genes, most of which play a role in mtDNA replication. Next generation sequencing led to the identification of compound heterozygous *RNASEH1* mutations in two simplex cases and a homozygous mutation in four siblings. *RNASEH1*, encoding ribonuclease H1, is an endonuclease present in both nucleus and mitochondria, which digests the RNA component of RNA/DNA hybrids. Unlike mitochondria, the nucleus harbours a second ribonuclease H activity (RNAseH2). All affected individuals started with CPEO and exercise intolerance in their twenties, followed by muscle weakness, dysphagia, and spino-cerebellar signs with impaired gait coordination, dysmetria and dysarthria. Ragged-red and COX negative fibres were observed in muscle biopsies of affected subjects' together with impaired activity of various mitochondrial respiratory chain complexes. Western blot analysis showed the virtual absence of the RNAseH1 protein in total lysate from mutant fibroblasts. By an in vitro assay, we demonstrated that mutant RNAseH1 variants have reduced capability to remove the RNA from RNA/DNA hybrids, confirming their pathogenic role. Since an increasing amount of evidence indicates the presence of RNA primers during mtDNA replication, this result may also explain the accumulation of mtDNA deletions and underscores the importance of RNAseH1 for mtDNA maintenance.

REPORT

Accumulation of multiple mtDNA deleted species (ΔmtDNA) in skeletal muscle and brain is the molecular hallmark of a group of autosomal recessive or dominant mitochondrial encephalomyopathies, characterized by chronic, progressive external ophthalmoplegia (CPEO) caused by mutations in nuclear genes affecting the integrity of the mitochondrial genome. This condition is part of a spectrum of clinically and genetically heterogeneous disorders of intergenomic communication, which also includes mtDNA depletion syndromes. An increasing number of genes have been associated with this category of mitochondrial disorders, encoding components of mtDNA replisome, mitochondrial deoxynucleotide supply, mitochondrial dynamics and quality control, and also proteins of still unknown function[1,2]. Recently, mutations in *DNA2* [MIM 601810][3] and *MGME1* [MIM 615076][4], encoding exonucleases involved in mtDNA repair or maturation, have been associated with CPEO/ΔmtDNA. We show here that mutations in *RNASEH1* [MIM 604123], encoding an endonuclease specific to RNA-DNA double stranded hybrids[5], cause the same syndrome. We studied two singleton subjects (S1, S2) and four affected siblings (S3-6) (Figure 1A). S1 and S2 developed juvenile-onset CPEO, muscle weakness and wasting, peripheral sensory-motor neuropathy, progressive spino-cerebellar ataxia and pyramidal signs. Involvement of respiratory muscles explains the severe nocturnal dyspnoea/orthopnoea in S1. CPEO occurred later in S3-6 siblings, but symptoms and progression were similar, with CPEO, dysphagia and respiratory impairment. S3, S4 and S5 died at 60, 70 and 63 years respectively; S6 is now 65 years old, wheelchair-bound, PEG-fed and under non-invasive ventilation. All affected individuals showed cerebellar involvement, secondary to MRI-proven cerebellar atrophy (Figure 1B). In

addition to CPEO, affected subjects displayed a number of peculiar features, e.g. exquisite involvement of respiratory muscles and progressive ataxia due to severe involvement of the spino-cerebellar pathways and cerebellar atrophy, which could be useful clues for diagnosis. Muscle biopsies of all six subjects showed numerous ragged-red, intensely SDH-positive, COX-negative fibres (Figure 1C). Electron microscopy on S2 muscle showed extremely elongated, hyperfused mitochondria (Figure 1D). Spectrophotometric analysis of S1 and S2 muscle homogenates, and S2 myoblasts, showed partially reduced complex I and IV activities, whereas values were normal in S1 fibroblasts. Detailed clinical and biochemical descriptions of the affected individuals are reported as supplemental case reports. Informed consent for participation in this study was obtained from all investigated subjects, in agreement with the Declaration of Helsinki and approved by the Ethical Committees of the Centers where biological samples were obtained. Southern-blot analysis showed multiple ΔmtDNAs in muscle from S1-4 and S6 (no muscle DNA was available for S5) (Figure 1E). The mtDNA copy number was unchanged (105% in S2) or increased (300% in S1) in skeletal muscle, while significant mtDNA depletion (16%) was detected in S2 myoblasts by qPCR (Figure 1F).

In order to identify the underlying genetic cause in our probands, we first ruled out several genes involved in CPEO/ΔmtDNA syndromes by Sanger' sequencing. We then performed whole-exome sequencing on S1 DNA; after filtering steps (Tables S1 and S2), we searched for homozygous or compound heterozygous variants, according to a recessive trait. From selected novel or rare variants in genes encoding known or predicted mitochondrial proteins, we zeroed on two changes in *RNASEH1* (RefSeq NM_002936.4), a c.424G>A (p.Val142Ile) on the paternal allele, and a nonsense c.469C>T (p.Arg157*) on the maternal allele. Next, we screened *RNASEH1* on a

cohort of 40 genetically undefined CPEO/ΔmtDNA individuals and identified compound heterozygous mutations c.424G>A (p.Val142Ile) and c.554C>T (p.Ala185Val) in S2. S3 was homozygous for the same p.Val142Ile found in S1 and S2; this mutation segregated with the disease, being homozygous in affected family members (Figure. 1A). All the identified *RNASEH1* variants were absent or extremely rare in public databases (<0.01% in ExAC; Table S3).

All amino acid changes map to the first third of the RNAseH1 catalytic domain (Figure 2A). The p.Arg157* affects the 22nd residue of the catalytic domain predicting the synthesis of a truncated protein species lacking catalytic activity as proven by in vitro assay (see below). Substitutions p.Val142Ile and p.Ala185Val affect amino acids close to conserved residues, part of the active site or interacting with RNA or DNA strands (Figure 2A).

RNASEH1 encodes mitochondrial and nuclear protein variants depending on which initiation AUG codons, encoding Met1 or Met27, are adopted. An upstream AUG, encoding Met0, competes with initiation at Met1, starting the mitochondrial variant, so that in physiological conditions the nuclear form, starting with Met27, is predominant[6]. An N-terminal MTS targets this protein to mitochondria, being eventually cleaved off by the mitochondrial matrix peptidase after translocation, resulting in a protein almost identical to the nuclear form. A second, exclusively nuclear ribonucleotidase activity on RNA:DNA hybrids is provided by RNAseH2, mutations in which are responsible of Aicardi-Goutieres syndrome [MIM 610333, 610181]. To circumvent potential cross contamination and demonstrate the effect of the *RNASEH1* mutations on protein activity, wild-type (wt) and mutant forms of mature human RNAseH1 were affinity-purified from overexpressing bacterial strains (Figures 1A and 1B). The *in vitro* activity of the recombinant proteins (Figure 2B)

was assessed on fluorescent-labeled oligos forming a 6 bp-long DNA:RNA heteroduplex (Figure S1B). Whilst the wt recombinant protein and *E. coli* RNaseH1 were both able to fully cleave the RNA from the heteroduplex, the recombinant mutants p.Val142Ile and p.Ala185Val displayed partial activity, leaving significant amount of intact single-stranded and incompletely cleaved oligos, similar to those obtained by incubating the wt protein with the heteroduplex on ice. Similar to the negative "no protein" control, recombinant truncated protein p.Arg157* showed negligible activity, as did the p.Asp210Asn mutant, previously reported as catalytically inactive[7] (Figure 2C).

To further investigate the molecular consequences of *RNASEH1* mutations, we characterized skin fibroblasts from S1 and two healthy control individuals, in permissive glycolytic-prone medium (containing glucose as the sole carbon source) or OXPHOS obligatory medium (containing galactose instead of glucose). *RNASEH1* transcript levels in S1 cells were decreased to 47% and 36% when grown in glucose or galactose, respectively (Figure S2), most likely due to nonsense-mediated mRNA decay of the transcript harbouring the premature stop codon. Western-blot analysis showed the virtual absence of the RNAseH1 protein in total S1 cell lysates (Figure 3A) suggesting instability of both RNAseH1^{Arg157*} and RNAseH1^{Val142Ile} variants. Whilst glucose-grown cells showed no significant differences, S1 cells grew slower in galactose than control cells (Figure 3B), suggesting mitochondrial dysfunction. Accordingly, cell cycle analysis revealed significant increase in G1/G0 and decreased S phases in galactose-grown S1 cells (Figure S3). To further assess mitochondrial dysfunction, we analysed mitochondrial morphology and membrane potential (ΔP) on live cells using TMRM and JC-1 immunofluorescence (Figure 3C). Glucose-grown S1 cells displayed a mitochondrial network similar to that of control cells, albeit the

intensity of the staining was significantly lower, indicating reduced ΔP (Figures 3C and S4A). Flow-cytometry analysis using JC-1 staining showed 50% ΔP decrease in S1 cells (Figure S4B). Whilst galactose-grown control cells showed neither alteration in mitochondrial morphology nor ΔP changes, S1 cells displayed perinuclear aggregation of fragmented mitochondria, (Figure 3C) and higher ΔP (Figure S4B).

To investigate the effect of *RNASEH1* mutations on mtDNA, we first analysed nucleoid structure in live cells from control and S1 fibroblasts by PicoGreen staining. Glucose-grown S1 fibroblasts displayed fewer, smaller and sharper nucleoids (Figures 3C and S5), whereas in galactose these differences were less prominent (Figure 3C), suggesting more active mtDNA metabolism in OXPHOS-obligatory conditions. Since PicoGreen staining is dependent on both amount and topology of mtDNA[8], and we had observed mtDNA depletion in S2S2 myoblasts, we further investigated mtDNA copy number by Southern-blot analysis. S1 fibroblasts showed mild (-20%) mtDNA depletion only in glucose and no ΔmtDNA was detected (Figures 4A and 4B). These results were confirmed by qPCR (Figure S6). However, we observed a >tenfold increase in 7S DNA (Figure 4C), the third strand of the mtDNA displacement loop (D-loop); mutant muscle also displayed higher levels of 7S DNA (Figure 4D), suggesting aborted replication.

Since these results indicated *RNASEH1* mutations to affect mtDNA replication, we studied replication intermediates by two-dimensional gel electrophoresis[9-11]. Glucose-grown S1 fibroblasts displayed a two- to four-fold increased signal compared to controls (Figures 5A-C and S7A). New replication intermediates, Y-arc extension, located at the end of the Y-arc pause, (Figures 5B and 5C), were detected in S1 fibroblasts. This extension of the Y-arc may originate by the presence of persisting RNA between the light-strand promoter and the conserved-sequence-block 1 or 2 that

would be removed in control fibroblasts by a well proficient RNAseH1 (Figure 5D)[11-13]. S1 fibroblasts also showed an increase in double-Y intermediates, indicating pausing at ribosomal genes, most likely owing to the failure of rRNA transcripts to be efficiently removed by mutant RNAseH1 (Figures 5B and 5D). Stronger signal in replication intermediates is consistent with replication slow-down, as also reported in *MGME1* mutations[4], and HEK cells overexpressing catalytic mutants of the mtDNA helicase or polymerase[14]. Galactose-grown cells showed decreased signal of almost all replication intermediates (Figure S7B). Finally, we performed mtDNA depletion and repopulation experiments. Glucose-grown cells exposed to the DNA intercalator EtBr for 96 hours, showed a decrease of mtDNA amount to <20% in all cell lines (Figure 6A). Whilst control cells recovered to initial mtDNA levels in 120 hours, S1 cells required 168 hours, indicating slower replication rate. Mutations in other genes involved in mtDNA replication such as *POLG1* [MIM 174763], *RRM2B* [MIM 604712] and *MGME1* have also been associated with slow or virtually no recovery in human fibroblasts[4; 15]. Active replication was measured as rate of BrdU incorporation in fibroblasts where nuclear replication was inhibited with aphidicolin (Figure 6B). S1 fibroblasts showed 30% less BrdU incorporation than control cells in both glucose and galactose media, indicating slower mtDNA replication in S1 fibroblasts, most likely due to stalling caused by RNA tracts not being efficiently removed by mutant RNAseH1[13; 16].

Our findings show that RNAseH1 is required for effective mtDNA replication in humans, as also suggested by embryolethality of an *Rnaseh1*$^{-/-}$ mouse model, which becomes virtually ρ^0 by p.c. 8.5[18]. Deleterious *RNASEH1* mutations slow down and stall mtDNA replication, causing both mtDNA depletion and deletions and ultimately leading to clinically overt mitochondrial disease. Unlike MGME1, which is

exclusively mitochondrial, and similar to DNA2, RNAseH1 is localized in both nucleus and mitochondria. Nevertheless its impairment determines a virtually exclusively mtDNA damage, most likely because of the compensatory role of nuclear RNAseH2. All three enzymes are involved in maturation of mtDNA and possibly in its repair, although RNAseH1 seems to play a direct important role in mtDNA replication by processing the RNA primers of nascent strands. This could also explain the accumulation of 7S DNA species, as defective RNAseH1 increases the proportion of intermediates with the 7S RNA still attached to the nascent H strand. This kind of molecules is poorly processed by MGME1[4] and that could result in aborted replication. FENMIT is an exclusively mitochondrial isoform of FEN1 [MIM 600393], that also interacts with RNA/DNA hybrids[19]. No mitochondrial diseases have been identified for FENMIT up to date and the degree of overlapping with RNAseH1 is not known. However, we could speculate that FENMIT could replace RNAseH1 in some instances and therefore, contributing to the mild phenotype in subjects with RNAseH1 mutations. According to the analysis of the replication intermediates by 2D-gel electrophoresis, mutant RNAseH1 is associated with increased pausing of the replication fork. Excessive pausing has been proposed as a mechanism leading to the accumulation of multiple deleted species and impairment of the replisome machinery either through breakage or recombination[20,21], which may also explain partial mtDNA depletion and slower recovery of mtDNA copy number associated with *RNASEH1* mutations.

Acknowledgments

We acknowledge the ‘‘Cell lines and DNA Bank of Paediatric Movement Disorders and Neurodegenerative Diseases’’ of the Telethon Network of Genetic Biobanks (grant GTB12001J) and the EurobiobanK Network. This work was supported by the Medical Research Council, the Pierfranco and Luisa Mariani Foundation, Telethon Grant GGP11011, the Italian Ministry of Health (GR2010–2316392 and ERC Advanced Grant FP7-322424.

Web Resources section

Online Mendelian Inheritance in Man (MIM): http://www.omim.org

Exome Aggregation Consortium (ExAC): http://exac.broadinstitute.org

References

1. Lamperti, C., and Zeviani, M. (2009). Encephalomyopathies caused by abnormal nuclear-mitochondrial intergenomic cross-talk. Acta Myol 28, 2-11.
2. Copeland, W.C. (2012). Defects in mitochondrial DNA replication and human disease. Crit Rev Biochem Mol Biol 47, 64-74.
3. Ronchi, D., Di Fonzo, A., Lin, W., Bordoni, A., Liu, C., Fassone, E., Pagliarani, S., Rizzuti, M., Zheng, L., Filosto, M., et al. (2013). Mutations in DNA2 link progressive myopathy to mitochondrial DNA instability. Am J Hum Genet 92, 293-300.
4. Kornblum, C., Nicholls, T.J., Haack, T.B., Scholer, S., Peeva, V., Danhauser, K., Hallmann, K., Zsurka, G., Rorbach, J., Iuso, A., et al. (2013). Loss-of-function mutations in MGME1 impair mtDNA replication and cause multisystemic mitochondrial disease. Nat Genet 45, 214-219.
5. Cerritelli, S.M., and Crouch, R.J. (1998). Cloning, expression, and mapping of ribonucleases H of human and mouse related to bacterial RNase HI. Genomics 53, 300-307.
6. Suzuki, Y., Holmes, J.B., Cerritelli, S.M., Sakhuja, K., Minczuk, M., Holt, I.J., and Crouch, R.J. (2010). An upstream open reading frame and the context of the two AUG codons affect the abundance of mitochondrial and nuclear RNase H1. Mol Cell Biol 30, 5123-5134.
7. Wu, H., Lima, W.F., and Crooke, S.T. (2001). Investigating the structure of human RNase H1 by site-directed mutagenesis. J Biol Chem 276, 23547-23553.
8. He, J., Cooper, H.M., Reyes, A., Di Re, M., Kazak, L., Wood, S.R., Mao, C.C., Fearnley, I.M., Walker, J.E., and Holt, I.J. (2012). Human C4orf14 interacts with the mitochondrial nucleoid and is involved in the biogenesis of the small mitochondrial ribosomal subunit. Nucleic Acids Res 40, 6097-6108.
9. Reyes, A., Yasukawa, T., Cluett, T.J., and Holt, I.J. (2009). Analysis of mitochondrial DNA by two-dimensional agarose gel electrophoresis. Methods Mol Biol 554, 15-35.
10. Di Re, M., Sembongi, H., He, J., Reyes, A., Yasukawa, T., Martinsson, P., Bailey, L.J., Goffart, S., Boyd-Kirkup, J.D., Wong, T.S., et al. (2009). The accessory subunit of mitochondrial DNA polymerase gamma determines the DNA content of mitochondrial nucleoids in human cultured cells. Nucleic Acids Res 37, 5701-5713.
11. Holt, I.J., and Reyes, A. (2012). Human mitochondrial DNA replication. Cold Spring Harb Perspect Biol 4.
12. Yasukawa, T., Reyes, A., Cluett, T.J., Yang, M.Y., Bowmaker, M., Jacobs, H.T., and Holt, I.J. (2006). Replication of vertebrate mitochondrial DNA entails transient ribonucleotide incorporation throughout the lagging strand. Embo J 25, 5358-5371.
13. Reyes, A., Kazak, L., Wood, S.R., Yasukawa, T., Jacobs, H.T., and Holt, I.J. (2013). Mitochondrial DNA replication proceeds via a 'bootlace' mechanism involving the incorporation of processed transcripts. Nucleic Acids Res 41, 5837-5850.
14. Wanrooij, S., Goffart, S., Pohjoismaki, J.L., Yasukawa, T., and Spelbrink, J.N. (2007). Expression of catalytic mutants of the mtDNA helicase Twinkle and

polymerase POLG causes distinct replication stalling phenotypes. Nucleic Acids Res 35, 3238-3251.
15. Stewart, J.D., Schoeler, S., Sitarz, K.S., Horvath, R., Hallmann, K., Pyle, A., Yu-Wai-Man, P., Taylor, R.W., Samuels, D.C., Kunz, W.S., et al. (2011). POLG mutations cause decreased mitochondrial DNA repopulation rates following induced depletion in human fibroblasts. Biochim Biophys Acta 1812, 321-325.
16. Pohjoismaki, J.L., Holmes, J.B., Wood, S.R., Yang, M.Y., Yasukawa, T., Reyes, A., Bailey, L.J., Cluett, T.J., Goffart, S., Willcox, S., et al. (2010). Mammalian mitochondrial DNA replication intermediates are essentially duplex but contain extensive tracts of RNA/DNA hybrid. J Mol Biol 397, 1144-1155.
17. Ruhanen, H., Ushakov, K., and Yasukawa, T. (2011). Involvement of DNA ligase III and ribonuclease H1 in mitochondrial DNA replication in cultured human cells. Biochim Biophys Acta 1813, 2000-2007.
18. Cerritelli, S.M., Frolova, E.G., Feng, C., Grinberg, A., Love, P.E., and Crouch, R.J. (2003). Failure to produce mitochondrial DNA results in embryonic lethality in Rnaseh1 null mice. Mol Cell 11, 807-815.
19. Kazak, L., Reyes, A., He, J., Wood, S.R., Brea-Calvo, G., Holen, T.T., and Holt, I.J. (2013). A cryptic targeting signal creates a mitochondrial FEN1 isoform with tailed R-Loop binding properties. PloS one 8, e62340.
20. Bailey, L.J., Cluett, T.J., Reyes, A., Prolla, T.A., Poulton, J., Leeuwenburgh, C., and Holt, I.J. (2009). Mice expressing an error-prone DNA polymerase in mitochondria display elevated replication pausing and chromosomal breakage at fragile sites of mitochondrial DNA. Nucleic Acids Res 37, 2327-2335.
21. Nicholls, T.J., Zsurka, G., Peeva, V., Scholer, S., Szczesny, R.J., Cysewski, D., Reyes, A., Kornblum, C., Sciacco, M., Moggio, M., et al. (2014). Linear mtDNA fragments and unusual mtDNA rearrangements associated with pathological deficiency of MGME1 exonuclease. Human molecular genetics 23, 6147-6162.
22. Alla, N.R., and Nicholson, A.W. (2012). Evidence for a dual functional role of a conserved histidine in RNA.DNA heteroduplex cleavage by human RNase H1. Febs J 279, 4492-4500.

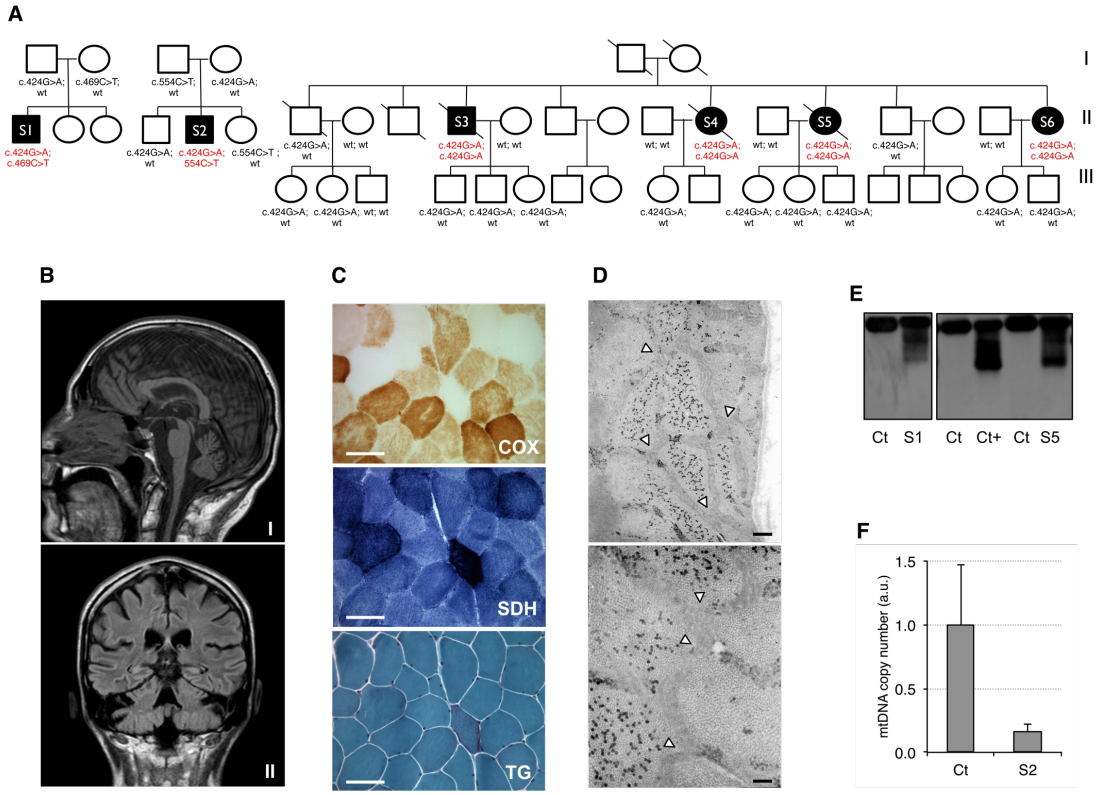

Figure 1. Clinical, morphological and genetic features of individuals with mutations in *RNASEH1*.

(A) Pedigrees of individuals with mutations in *RNASEH1*. Black symbols designate affected subjects, numbered according to the main text. The mutation status of all analysed family members is indicated, based on *RNASEH1* RefSeq.

(B) Brain MRI in subject 1. T1 sagittal (panel I) and cross (panel II) sections showing cerebellar atrophy and mild bulbar atrophy in S1.

(C) Histological findings in subject 2 muscle biopsy: Cytochrome c oxidase (COX), succinate dehydrogenase (SDH), Gomori Trichrome (GT) staining showing 1 ragged-red COX-/SDH+ fiber and several COX- fibers (Scale bars: 25μm).

(D) Electron microscopy with seamless mitochondrial network intermingled among myofibrils in subject 2 (S2) muscle biopsy (Arrowheads indicate ramification of the mitochondrial syncytium. Scale bars: 0.25 μm upper panel; 0.10 μm lower panel).

(E) Southern blot analysis of mtDNA obtained from muscle biopsies of affected individuals 1 and 5 (S1, S5), of control subjects (Ct) and of an individual with *POLG1* mutations (Ct+).

(F) mtDNA levels assessed by qPCR in myoblasts from subject 2 (S2) and three controls (Ct). The mean value of the ratio mtDNA/nDNA obtained in controls was set as 1. Error bars represent standard deviations.

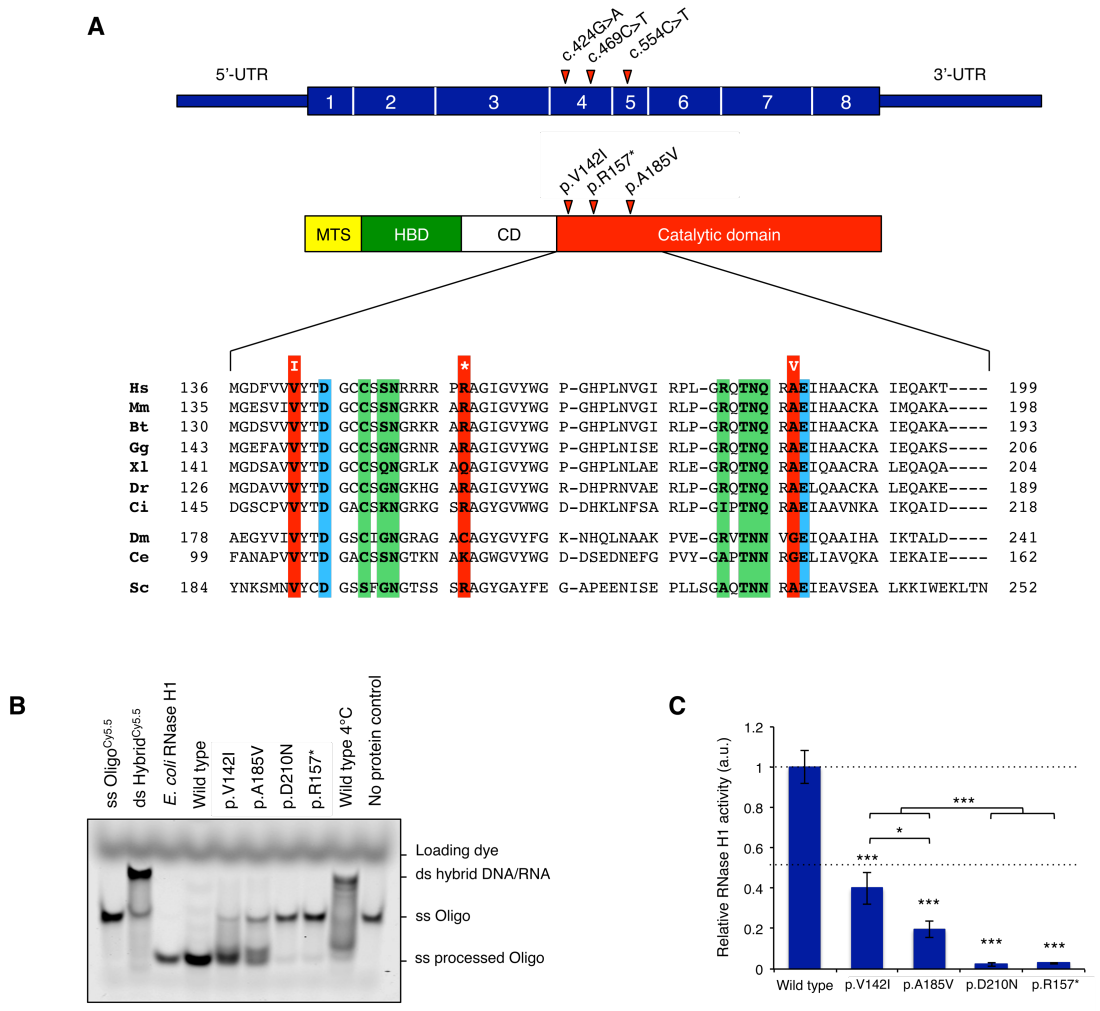

Figure 2. Characterization of the structure and enzymatic activity of *RNASEH1* variants.

(A) Human RNAseH1 (top) consists of four domains: a mitochondrial targeting sequence (MTS) that directs the protein to mitochondria and is cleaved after import, a hybrid binding domain (HBD) involved in recognition of DNA·RNA heteroduplexes, a catalytic domain responsible for the cleavage of the RNA component in the heteroduplex, and a flexible connection domain (CD) that links the last two domains. Phylogenetic alignment of the human protein region containing the substitutions found in affected individuals is shown below. Conserved residues mutated in affected subjects are boxed in red and are found near conserved residues in the active site or interacting with DNA or RNA in the heteroduplex, boxed in blue or green,

respectively. Hs, *H. sapiens*; Mm, *M. musculus*; Bt, *B. taurus*; Gg, *G. gallus*; Xl, *X. laevis*; Dr, *D. rerio*; Ci, *C. intestinalis*; Dm, *D. melanogaster*; Ce, *C. elegans*; Sc, *S. cerevisiae*.

(B) RNAseH1 activity of recombinant proteins. The portion corresponding to the mature protein, lacking the mitochondrial targeting signal (MTS), was cloned into pET-28a bacterial expression vector (Novagen) which contains a N-terminal His_6 tag. Protein expression was carried out in BL21(DE3)pLysS *E. coli* cells at 37ºC in LB medium. Proteins were loaded onto a Ni-NTA agarose column and eluted with 400 mM imidazole. 80 nmoles of DNA·RNA heteroduplex oligo were incubated with either *E. coli* RNAseH1 or either wild type or mutant recombinant proteins for 1 hour[22]. Reaction products were loaded onto 15% polyacrylamide gels followed by gel imaging and quantification.

(C) Relative RNAseH1 activity was obtained by quantifying the amount of processed oligo normalized by protein loading (based on Western blotting, Supplementary Fig. 1c) and relative to wild type protein. $*P < 0.05$, $***P < 0.001$; two-tailed unpaired Student's *t* test; $n = 3$; error bars = 1 s.d.

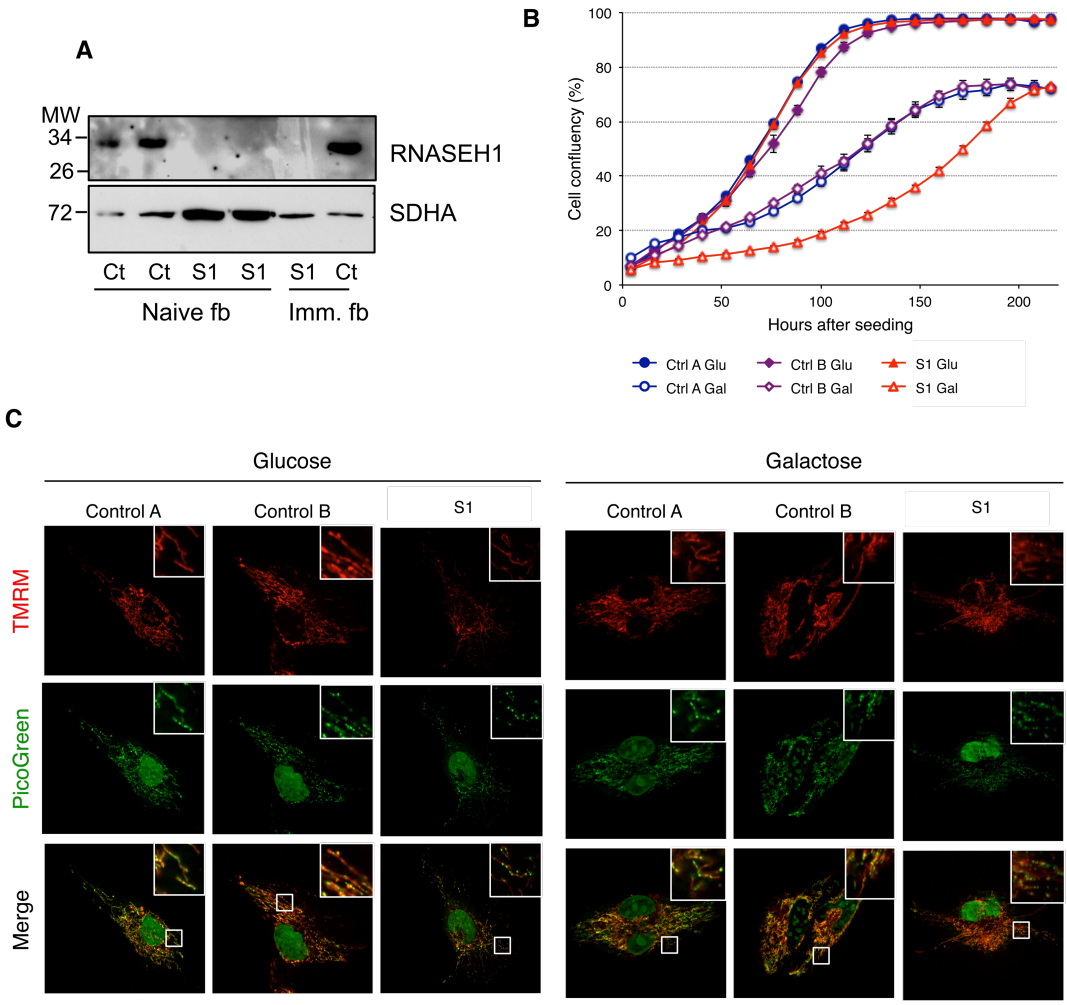

Figure 3. Growth and mitochondrial alterations in *RNASEH1* mutant fibroblasts.

(A) Western Blot analysis of fibroblasts (fb) from affected subject 1 (S1) and controls (Ct) using antibodies against RNASEH1 (Abcam) and SDHA (Mitosciences-Invitrogen); the latter was taken as a loading control. Both naïve and immortalized (Imm.) fibroblasts were used.

(B) Growth curves of control and *RNASEH1* S1 cells in glucose (high-glucose medium) and galactose (glucose-free medium supplemented with 50mM galactose). Cell growth was monitored continuously by IncuCyte live cell imager (Essen Bioscience). Data are shown as average and s.d. of three independent experiments.

(C) Mitochondria (red) were stained for 20 min with *ΔP*-dependent dye, TMRM (20 nM), and DNA (green) with PicoGreen (3 μl/ml) in live cells grown in glucose or galactose for 5 days. Digitally enhanced TMRM image from *RNASEH1* mutant fibroblasts from S1 is shown in Figure S4A.

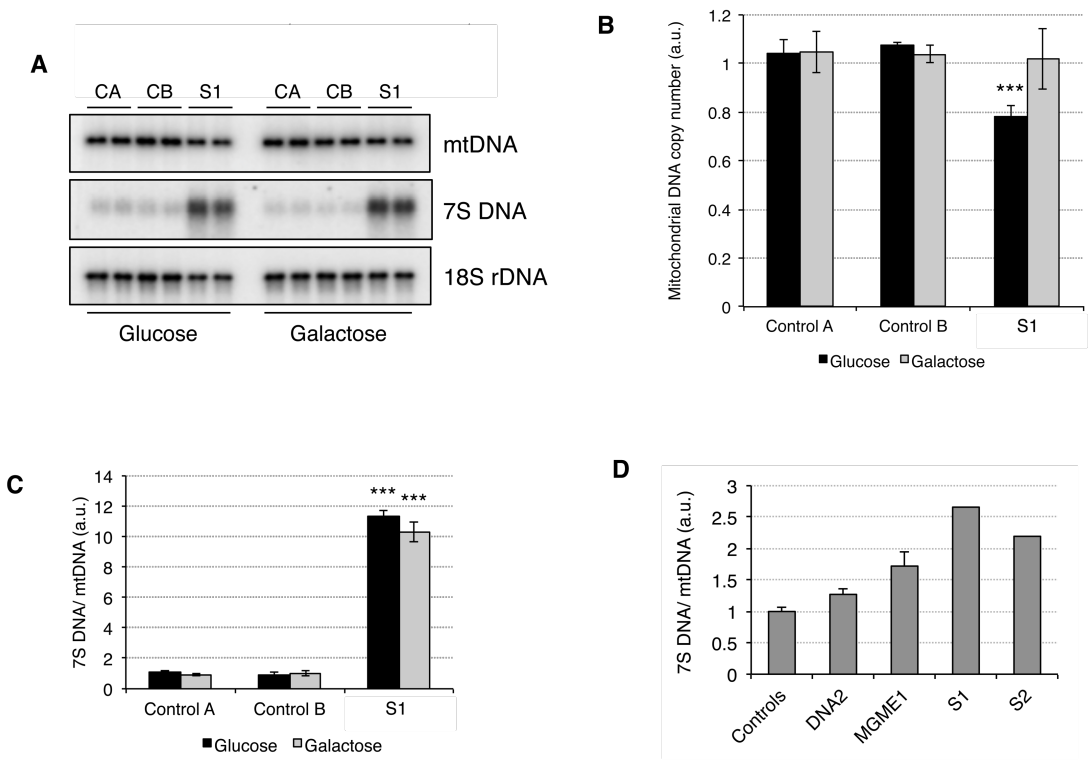

Figure 4. Mitochondrial DNA copy number and 7S DNA alterations in *RNASEH1* mutant fibroblasts from S1 and muscle from S1 and S2.

(A) Total DNA from control and *RNASEH1* mutant fibroblasts was digested with *Pvu*II and mtDNA was analysed by one-dimensional Southern blot. Radioactive probes specific for the human mtDNA D-loop region (nucleotide positions 16.341-16.151, able to detect both linearised mtDNA and 7S DNA) and 18S ribosomal DNA were applied.

(B) Relative mtDNA copy number (mtDNA/18S rDNA ratio) was obtained after quantification of the Southern-blot signal with PhosphorImager screens and normalization to control fibroblasts. ***$P < 0.001$; two-tailed Student's t test; $n = 2$; error bars = 1 s.d.

(C) 7S DNA levels (7S DNA/mtDNA ratio) were obtained after quantification of the Southern-blot signal with PhosphorImager screens and normalization to control fibroblasts. ***$P < 0.001$; two-tailed Student's t test; $n = 2$; error bars = 1 s.d.

(D) 7S DNA levels (7S DNA/mtDNA ratio) in muscle from S1, S2 and subjects with mutations in *MGME1* and *DNA2* assessed by qPCR.

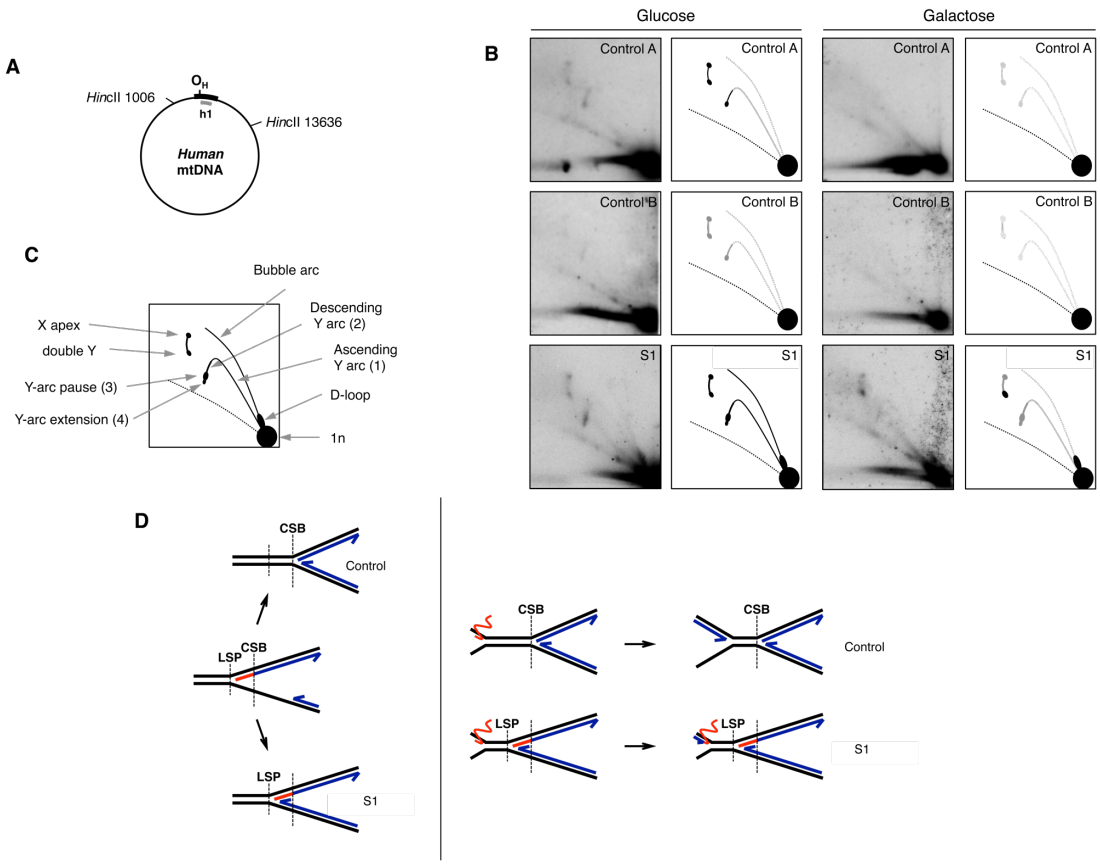

Figure 5. Effect of mutant *RNASEH1* fibroblasts from S1 on mtDNA replication.

(A) Restriction enzyme sites and position of the probe are labeled. The origin of the H-strand replication (O_H) is marked within the non-coding region (black bar).

(B) mtDNA replication intermediates analysed by two-dimensional agarose gel electrophoresis (2D-AGE) and Southern bot. Explanatory cartoons are provided at the right of each image, with shades of gray reflecting the different intensities of the signal.

(C) A cartoon based on this and previous work[9-13] shows different replication intermediates associated to this fragment and the non-replicating fragment, 1n.

(D) Proposed models that could explain the presence of a Y-arc extension (left) and increased double Y (right) mtDNA replication intermediates from *RNASEH1* mutant fibroblasts from S1. Parental DNA strands are in black, nascent DNA strands in blue

and RNA in red. L-strand promoter (LSP) and conserved sequence block region (CSB) are marked as reference points.

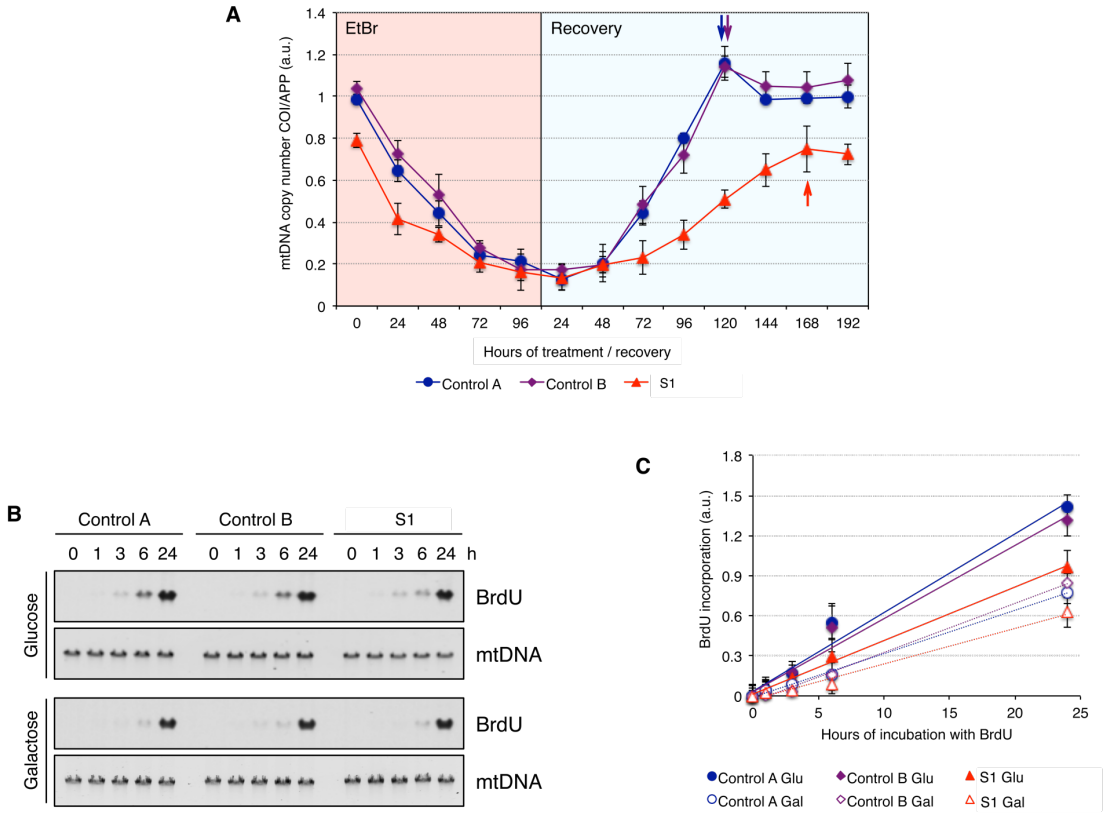

Figure 6. MtDNA replication is slowed down in mutant *RNASEH1* fibroblasts from S1.

(A) mtDNA copy number during depletion and recovery in control and *RNASEH1* mutant fibroblasts. Depletion was achieved by addition of 100 ng/ml EtBr to the culture medium for 96 h and recovery was followed up for 192 h after the removal of the drug. The mtDNA copy number was determined by qPCR, each data point representing the mean values from two independent determinations ± s.d. Arrowheads indicate the time point at which mtDNA was recovered at or close to initial values for each cell line.

(B) Detection of newly synthesized mtDNA. Cells were treated with 20 μM Aphidicolin (Sigma) for six hours to block nuclear DNA replication. Total DNA from control and *RNASEH1* mutant fibroblasts subjected to pulse-labeling of mtDNA with BrdU (100 μM) for 0, 1, 3, 6 and 24 h was digested with *Nae*I and analysed by one-dimensional Southwestern blot. BrdU signal was immonodetected with anti-BrdU

antibody (Becton Dickinson) and was followed by mtDNA detection using a radioactive probe specific for the human mtDNA D-loop region.

(**C**) Plot of BrdU incorporation over time, normalized to mtDNA loading; the linear regression for each cell line is shown. Each data point represents the mean of two replicates ± s.d.

Supplemental Case Reports

Subject 1

Subject 1 (S1) is a 42 year old male born after uncomplicated pregnancy and delivery, from healthy unrelated parents. He has two healthy daughters. His psychomotor development was normal. At 20 years of age he started complaining of muscle pain and at 21 he noticed eyelid ptosis associated with progressive ophthalmoplegia, occasional dysphagia, speech difficulties, and postural instability. At neurological examination he showed CPEO, dysarthria, dysphonia, wide-based gait, exercise intolerance with muscle cramps and weakness, particularly affecting the lower limbs. Neither hearing loss nor cardiac abnormalities nor diabetes were reported. Bilateral eyelid ptosis required surgery at the age of 32. At 36 he experienced recurrent episodes of ventilatory insufficiency including nocturnal dyspnoea and orthopnea; an acute episode required tracheostomy. He nevertheless recovered from this condition and later respiratory assessment disclosed only a mild restrictive deficit, without sleep apnoea, dyspnoea or orthopnea (average nocturnal oxygen saturation about 90%). ECG and Echocardiogram were normal. Laboratory tests showed high CK levels (400 U/L; normal values, n.v. <195) and mild lactate increase (2856 μmol/L; n.v. 580-2100). Brain MRI revealed moderate cerebellar and brain stem atrophy. A neurophysiologic assessment was performed: an Electromyography (EMG) showed mild motor demyelinating neuropathy prevalent in the lower limbs, eyelid and distal myopathic signs; Multimodal Evoked Potentials: multisystem CNS involvement with particularly altered Somatosensory evoked potentials (SEP) in the lower limbs.

A muscle biopsy showed numerous ragged-red and COX negative fibres. Respiratory chain analysis performed on muscle tissue showed partial reduction of complex I and IV activity; the same analysis did not show alteration when performed on S1 skin fibroblasts.

In the last few years, S1 experienced mild worsening of standing and gait stability, while muscle weakness and ventilatory impairment are stable.

Subject 2

Subject 2 (S2), a 46 year old man, is the second child of healthy non consanguineous parents. Family history was negative for neurological diseases; his motor

development was normal and he had a regular scholastic course. He had no neuromuscular abnormalities until 23 years of age, when he developed a progressive bilateral ptosis without diplopia. Neurological examination showed lateral and up gaze ophthalmoplegia, brisk reflexes with distal clonus and bilateral extensory plantar response. He referred fatigability, with no dyspnoea, dysphonia or dysphagia. The laboratory examination of plasma gave normal results with the only exception of increased lactate (30.8 mg/dl; n.v. 5.7-22 mg/dl). The EMG showed mild neurogenic signs; the EEG indicated generalized slow wave activity, with paroxysmal bilateral graphoelements, enhanced by hyperpnoea. An Echocardiogram (ECG) showed right bundle branch block pattern; fundus oculi and audiometry were normal. CSF investigation showed no pathological issues. MRI study was refused because of claustrophobia. Histological examination on biceps muscle biopsy displayed ragged red fibres (RRF) and absence of COX activity in several scattered fibres, many of which also showing intense SDH-positivity. Spectrophotometric analysis of MRC complex activities normalized to citrate synthase (CS) showed decreased cIV/CS ratio in muscle homogenate and in myoblasts (55% of control mean in both specimens), with partial reduction of cI+cIII/CS ratio (62%). Over the following 20 years, S2 experienced worsening of ocular movements and muscle weakness. At the latest neurological examination (45 years of age) he presented severe gait impairment, being now unable to walk long distance, needing a wheelchair. Progressive head drop, dysphagia and trunk weakness had ensued. He also presented decreased visual acuity (5/10 right, 2/10 left), a complete ophthalmoplegia and profound weakness of orbicular oris and oculi muscles leading to corneal lesions with neovascularization. Other features included hypotrophy of interossei and thenar eminence, moderate limb (MRC 3-4/5) and marked axial muscle weakness (MRC 2-3/5), with tendency to propulsion of head and trunk. Mild cerebellar signs in the upper limbs were present; tendon reflexes were decreased, sensory examination showed isolated impairment of discriminative perception. Visual evoked potentials were undetectable. Electroretinogram showed reduction in amplitude. The subject developed arterial hypertension without respiratory and cardiologic involvement.

Siblings S3-6

Subject 5 (S5) was born after uncomplicated pregnancy and delivery from healthy related parents. The same clinical phenotype was reported in three siblings (S3, S4, S6) while other four siblings were unaffected (Fig. 1a). She had two daughters and one son, all healthy. At 45 years old she started complaining of eyelid ptosis and ophthalmoparesis. The symptoms worsened progressively and she started presenting dysphonia, dysphagia leading to significant weight loss, and walking difficulties. The clinical examination at 48 years showed CPEO with paraparetic gait associated with pyramidal signs, and increased deep tendon reflexes. Some cerebellar signs were noticed such as dysmetria and a positive Romberg sign. Cognitive impairment and motor slowing were present. A brain MRI showed cerebellar and cortical atrophy with hyper-intense lesions in the deep periventricular white matter. She did not report hearing loss. The EMG pattern showed diffuse, proximal neuropathy. Cardiologic assessment was normal (ECG) at 48 years of age. CK levels were reported as normal. A muscle biopsy performed at the age of 48 showed ragged-red and COX negative fibres. She died at the age of 63 years for a sudden cardiac event.

Her younger sister (S6), now aged 65, had a similar disease history. She started at 40 years presenting with CPEO associated with progressive gait instability, severe dysphagia and ventilatory impairment. A muscle biopsy performed at 40 years showed mitochondrial myopathy (ragged red and COX negative fibers). She is now wheelchair bound, receives nutrients through a percutaneous endoscopic gastrostomy (PEG) and needs ventilatory support (non-invasive ventilation, NIV) during the day and oxygen administration during the night.

A second sister (S4) died at 70 years because of respiratory failure and an older brother (S3) died at 60 years of unknown cause. Both were reported to have suffered of a similar condition with CPEO, dysphagia and respiratory impairment.

Figure S1: **Recombinant RNAseH1 protein purification and *in vitro* assay**

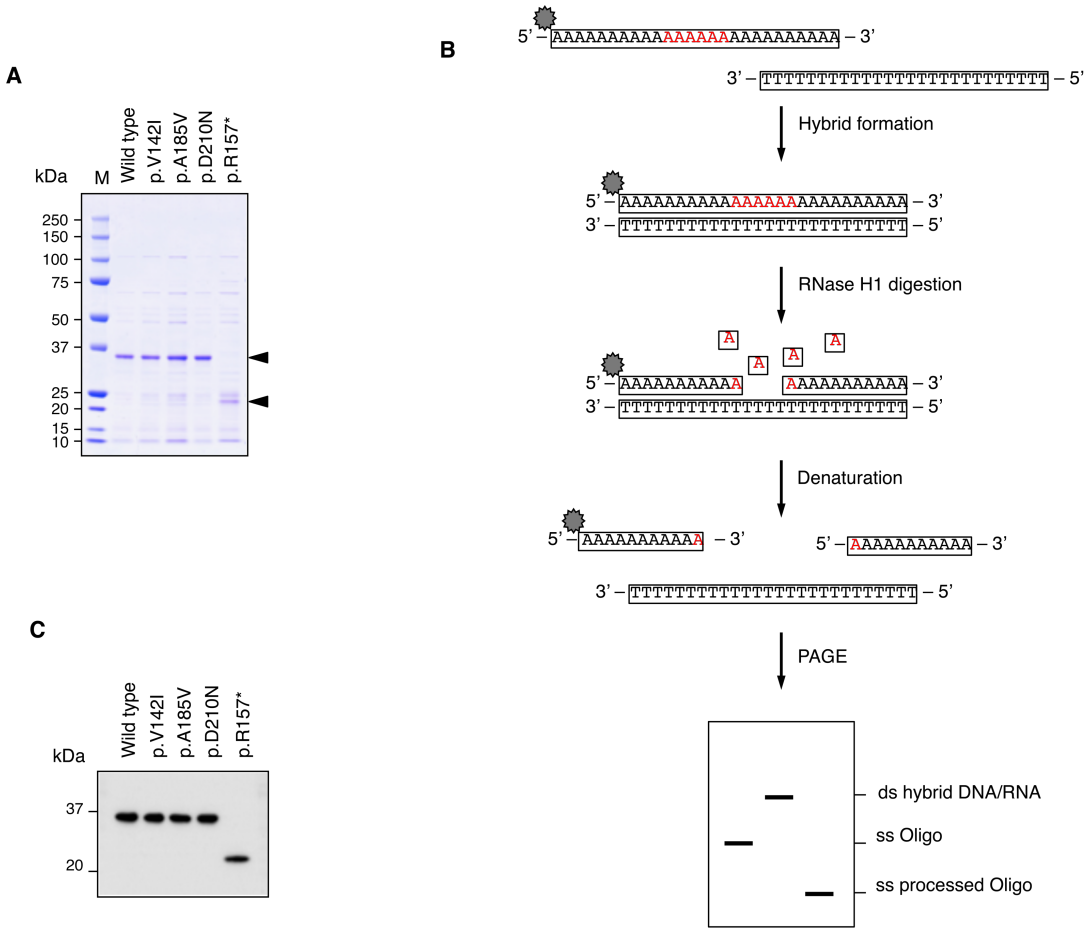

(A) SDS-PAGE gel stained with Coomassie Brilliant Blue showing the protein profile of eluted fractions with 400 mM imidazole from the affinity purification of wt and mutant HIS.RNASEH1.HIS. The most intense protein bands (marked with arrowheads) of ~37 and ~21 kDa correspond to the purified HIS.RNASEH1.HIS protein.
(B) In vitro assay for the measurement of RNAseH1 activity. A 5' end Cy5.5 fluorescently labelled chimeric oligo $dA_{10}A_6dA_{10}$ was hybridised to an oligo dT_{26} and incubated at 37ºC for 1h. In the presence of active RNAseH1, the RNA component of the heteroduplex is cleaved. Then, loading buffer containing formamide was added and samples boiled at 85ºC for 5 min, and then cooled on ice before loading onto 15% polyacrylamide gels in 1xTBE. This will produce a processed fragment of shorter length but still labelled at the 5' end and clearly distinguishable from the non-cleaved oligo used to form the heteroduplex. Control heteroduplex was not denatured before loading to avoid separation of the two strands and is loaded only as reference.
(**C**) The identity of the purified proteins was confirmed by Western blotting with anti-His antibody. These Western blots were also used as loading control for the normalization of the in vitro activity shown in **Figure 1C**.

Figure S2: ***RNASEH1*** **transcript levels**

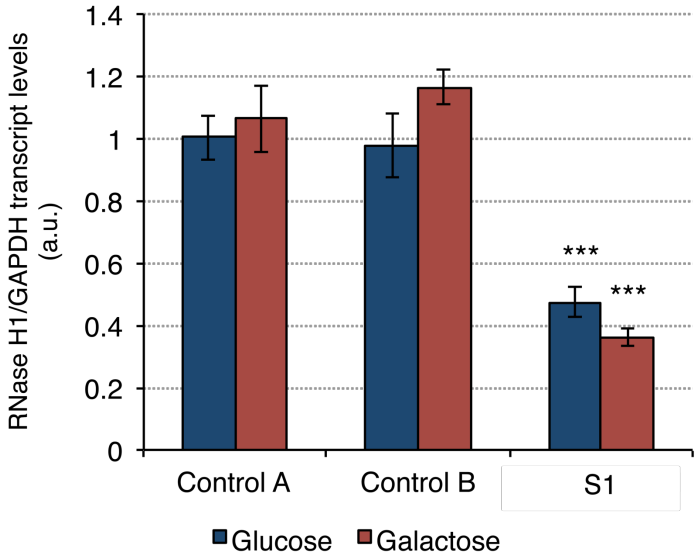

Transcript levels were investigated with Life Technologies Gene Expression Assay (Hs00268000_m1) and normalized to GAPDH (Hs02758991_g1). Cells were grown in either glucose or galactose for five days. ***$P < 0.001$; two-tailed Student's t test; $n = 2$; error bars = 1 s.d.

Figure S3: **Cell cycle analysis**

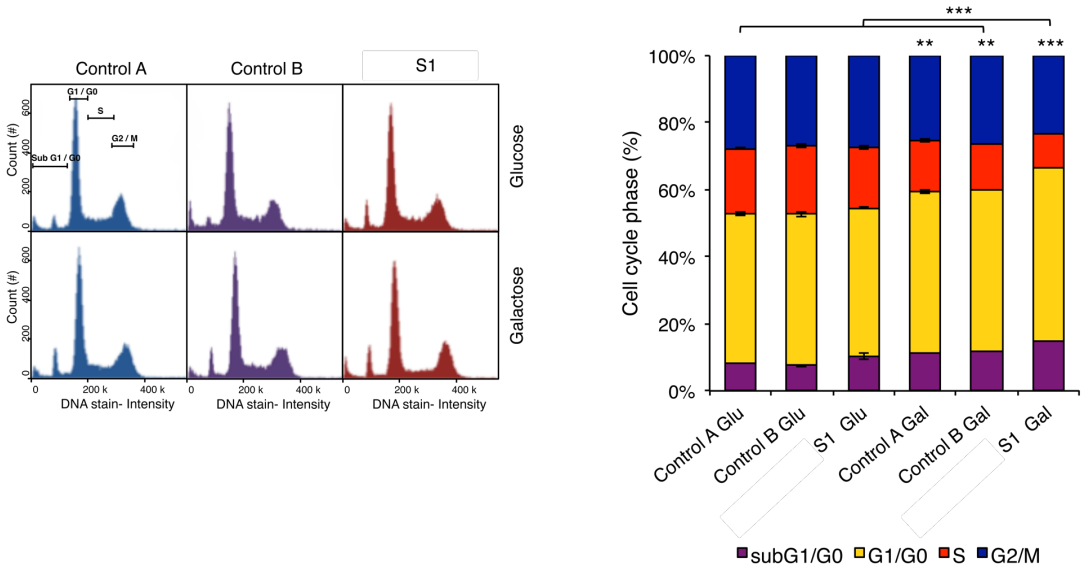

Control and mutant fibroblasts grown in glucose or galactose for five days were subjected to cell cycle analysis using propidium iodine (left). The proportion of cells in sub G1/G0, G1/G0, S and G2/M phases was scored for each sample (right). $^{**}P < 0.01$, $^{***}P < 0.001$; two-tailed Student's *t* test; $n = 4$; error bars = 1 s.d.

Figure S4: **Mitochondrial membrane potential**

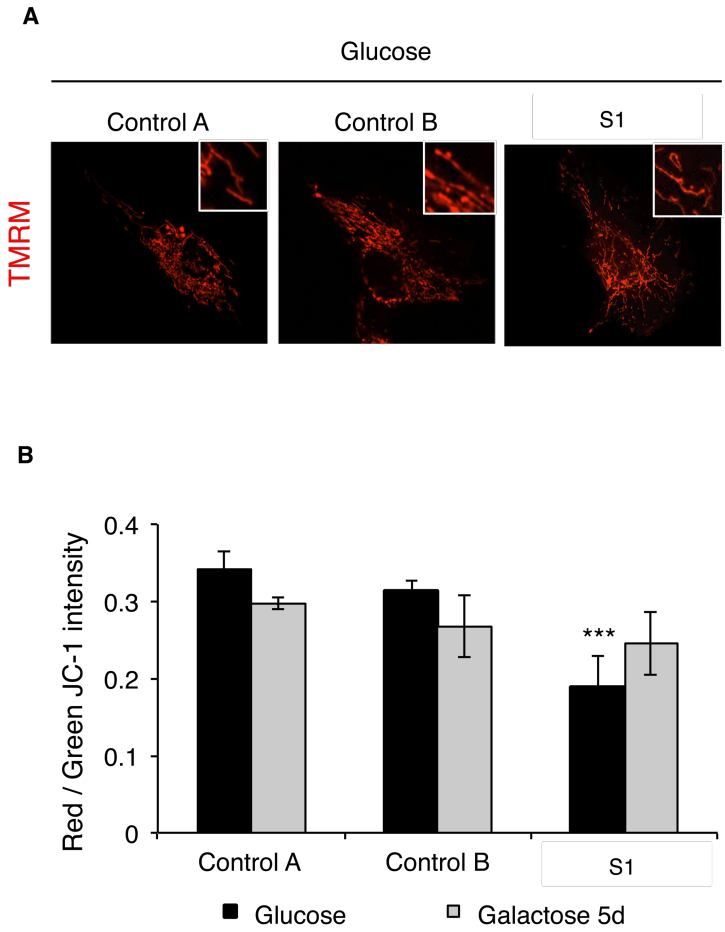

(A) TMRM staining of live cells grown in glucose for five days as shown in **Figure 2B** was indicative of lower membrane potential in mutant fibroblast. However, the low signal did not allow a proper comparison of the mitochondrial morphology. Therefore, the signal has been two-fold enhanced in the *RNASEH1* mutant fibroblasts in order to better appreciate the mitochondrial network. No significant difference compared to controls is observed.
(B) Quantification of mitochondrial membrane potential in fibroblasts grown in glucose or galactose for five days using JC-1 staining. The ratio of red to green JC-1 is plotted for the different samples as a measure of mitochondrial membrane potential. ***$P < 0.001$; two-tailed unpaired Student's t test; $n = 4$; error bars = 1 s.d.

Figure S5: **Nucleoid measurements**

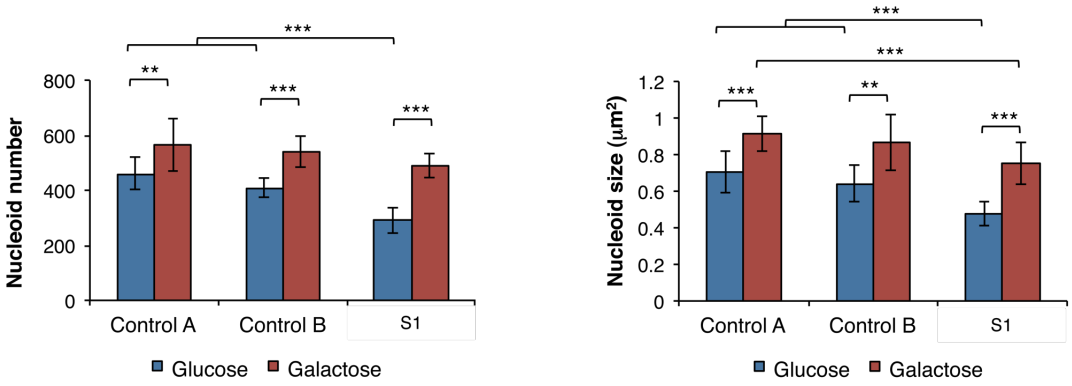

Nucleoid number (left) and size (right) were quantified in live cells grown in glucose or galactose for five days and stained with PicoGreen. Cells were imaged with a ZEISS ApoTome fluorescence microscope using a 40X immersion objective. Analysis was carried out using Particle Counting application available in ImageJ. $^{**}P < 0.01$; $^{***}P < 0.001$; two-tailed Student's *t* test; $n = 10$; error bars = 1 s.d.

Figure S6: **Mitochondrial DNA copy number**

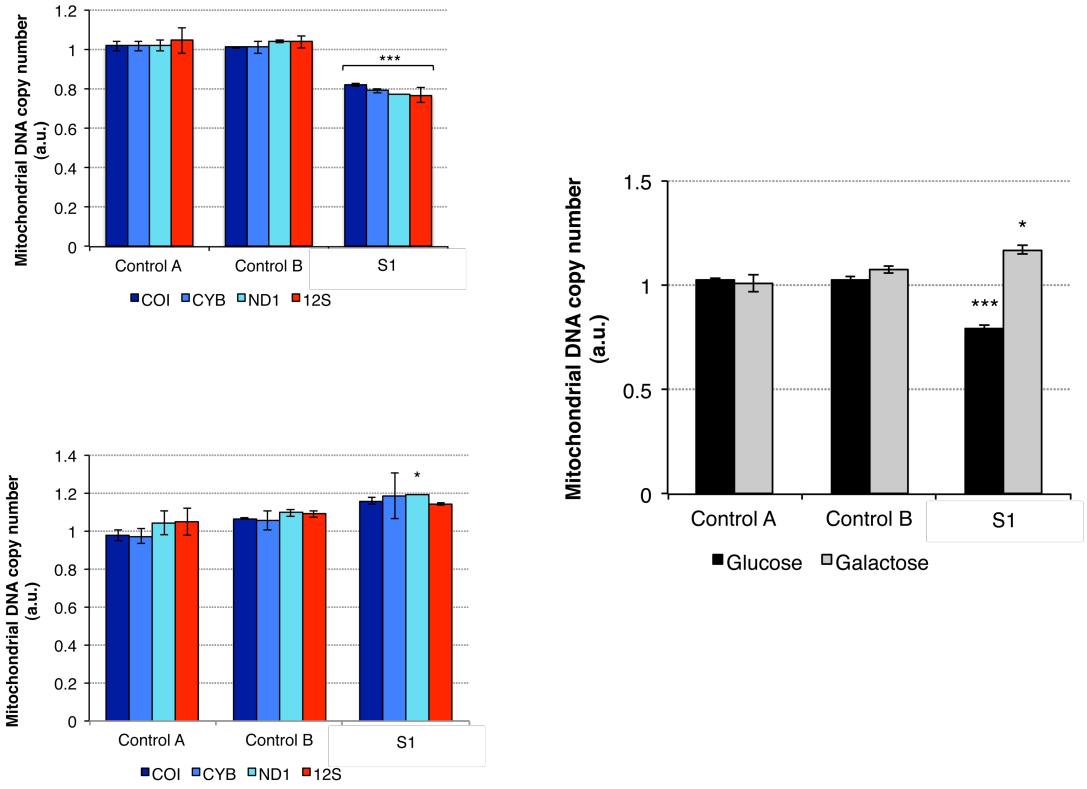

Relative mtDNA copy number was assessed in cells grown in glucose (top left) or galactose (bottom left) for five days by qPCR using Life Technologies Gene Expression Assays for four mitochondrial genes: COI (Hs02596864_g1), CYB (Hs02596867_s1), ND1 (Hs02596873_s1) and 12S rDNA (H202596859) and normalized to APP (Hs02339796_cn) levels. Control cells grown in glucose were arbitrarily chosen as reference and given value 1. Average of all four mitochondrial genes are shown on the right. *$P < 0.05$; ***$P < 0.001$; two-tailed unpaired Student's t test; $n = 4$; error bars = 1 s.d.

Figure S7: **Quantification of replication intermediates from 2D-AGE**

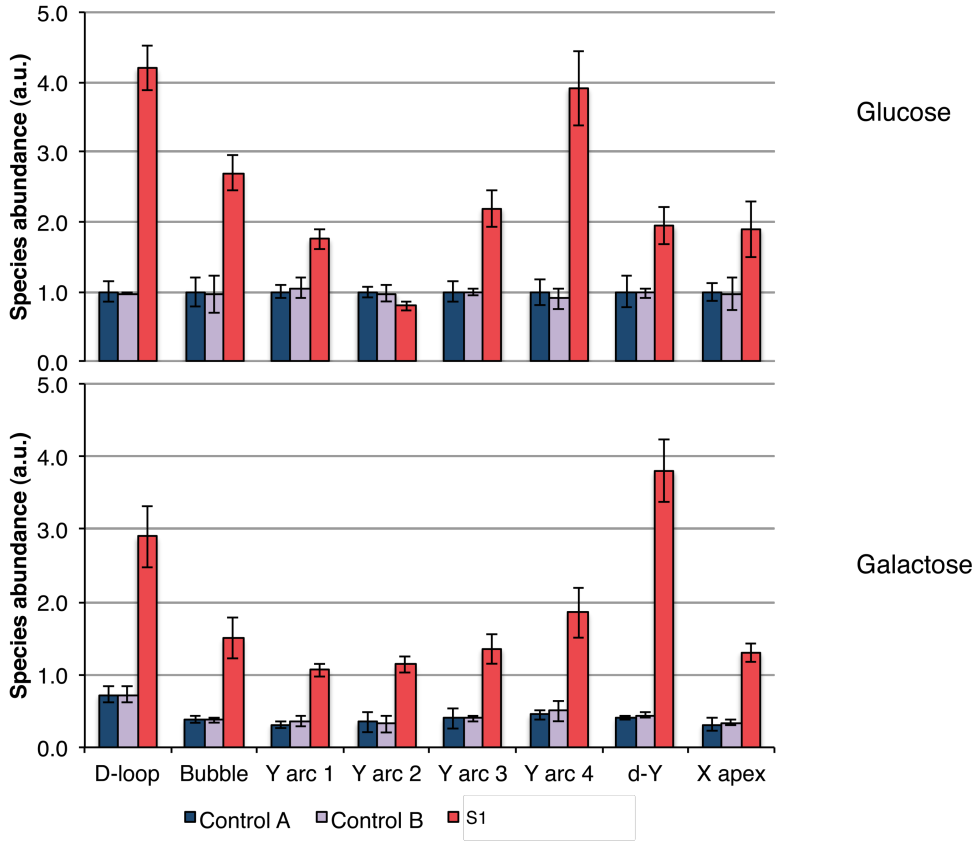

Replication intermediates and non-replicating mtDNA (1n) from cells growing in glucose or galactose for five days and shown in **Figure 2A** were quantified using ImageQuant software and normalized to the amount of non-replicating molecules (1n) for each sample. Control cells grown in glucose were arbitrarily chosen as reference and given value 1. ***$P < 0.001$; two-tailed unpaired Student's t test; $n = 2$; error bars = 1 s.d.

Table S1: Functional variants number filtered by public databases. The functions of variants include missense, readthrough, nonsense, spliceSite, 5'-UTR and 3'-UTR.

Filter method	**Functional variants (SNP+InDel)***
Before filtering	18,014+1,826
Filtered by 1000 Genome variants database	1,808+519
Filtered by 1000 Genome variants database_ HapMap	1,333+308
Filtered by 1000 Genome variants database_ HapMap_ESP	1,317+308

* SOAPaligner/SOAP2 (soap2.21) was use for mapping clean reads onto human reference genome (UCSC hg19, build 37.1), and SOAPsnp (v. 1.03) was used for SNP calling. BWA was used for mapping reads onto reference sequence in InDel analysis, and GATK (Genome Analysis Tool Kit) was used for InDel detection.

Table S2: Prioritization of candidate genes

Filter method	**Genes**
Recessive trait (≥2 variants/gene)	118
Only coding and splice-site variants	26
Predicted mitochondrial localization*	3 (*AGXT*, *RNASEH1*, *TIMM23*)

* Maestro score >0 (www.broadinstitute.org)

Table S3: *RNASEH1* mutations

Subject	DNA	Protein	Father/ Mother	Exac frequency	In vitro activity [a]	M
S1	c.424G>A	p.Val142Ile	F	0.00004963	40%	Di
	c.469C>T	p.Arg157*	M	0.000008255	5%	Di
S2	c.554C>T	p.Ala185Val	F	n.r.	20%	Di
	c.424G>A	p. Val142Ile	M	0.00004963	40%	Di
S3-6	c.424G>A	p. Val142Ile	F	0.00004963	40%	Di
	c.424G>A	p. Val142Ile	M	0.00004963	40%	Di

Nomenclature according to HGVS (NM_002936.4; NP_002927.2). F, father; M, mother. n.r.: not reported. [a]: compared to the activity of the wild-type enzyme.
[b]: http://www.mutationtaster.org (Disease= disease causing)
[c]: http://genetics.bwh.harvard.edu/pph2 (Damaging=probably damaging)